COMBINING BINARY DECISION TREE AND GEOSTATISTICAL METHODS TO ESTIMATE SNOW DISTRIBUTION IN A MOUNTAIN WATERSHED

Benjamin Balk[1,2] and Kelly Elder[1]

ABSTRACT

We model the spatial distribution of snow across a mountain basin using an approach that combines binary decision tree and geostatistical techniques. In April 1997 and 1998, intensive snow surveys were conducted in the 6.9 km^2 Loch Vale watershed (LVWS), Rocky Mountain National Park, Colorado. Binary decision trees were used to model the large-scale variations in snow depth while the small-scale variations were modeled through kriging interpolation methods. Binary decision trees related depth to the physically based independent variables of net solar radiation, elevation, slope and vegetation cover type. These decision tree models explained 54-65% of the observed variance in the depth measurements. The tree-based modeled depths were then subtracted from the measured depths, and the resulting residuals were spatially distributed across LVWS through kriging techniques. The kriged estimates of the residuals were added to the tree-based modeled depths to produce a combined depth model. The combined depth estimates explained 60-85% of the variance in the measured depths. Snow densities were mapped across LVWS using regression analysis. Snow-covered area (SCA) was determined from high-resolution aerial photographs. Combining the modeled depths and densities with a snow cover map produced estimates of the spatial distribution of snow water equivalence (SWE). This modeling approach offers improvement over previous methods of estimating SWE distribution in mountain basins.

INTRODUCTION

Ensuring adequate water supplies is the crux of many political, economic, social and environmental debates, particularly in the arid American West. A major source of water in the American West is the seasonal accumulation of snow in mountain basins. Snowmelt runoff from mountainous regions contributes about 75% of the streamflow in the western United States [*Doesken and Judson*, 1996]. Downstream agricultural, municipal, industrial and recreational interests greatly depend on this snowmelt runoff to meet their demands.

The development of physically based, spatially distributed snowmelt models requires better estimates of the spatial distribution of SWE. *Blöschl et al.* [1991] demonstrated that a solid understanding of SWE distribution is crucial for realistic predictions of the spatial characteristics of the snowmelt process. SWE distribution is a dominant factor in the timing of runoff as certain areas of mountain basins may generate snowmelt more rapidly than other areas. Energy exchanges, topographical characteristics, surface roughness and wind redistribution contribute to the spatial heterogeneity of mountain snowpacks, particularly snow depth and SWE [*Elder et al.*, 1991], and complicate efforts to model snow distribution.

Although snow-covered area (SCA) can be mapped from operational remote sensing platforms, the use of remote sensing alone to directly measure SWE is not feasible. Measurements of the spatial distribution of basin-wide SWE must be performed by intensive field sampling to capture the large spatial variability of mountain snowpacks [*Cline et al.*, 1998]. The interpolation of ground-based point measurements, therefore, becomes imperative to understand the spatial distribution of SWE over an entire drainage basin. Research efforts using binary decision tree methods to distribute measured values of SWE over mountain watersheds have proved promising [*Elder*, 1995; *Elder et al.*, 1998]. Geostatistical techniques have also been applied to estimate basin-wide SWE [*Hosang and Dettwiler*, 1991; *Balk et al.*, 1998]. For this study in a small mid-latitude mountain basin, we modeled the large-scale variability of snow depth through binary decision trees and the small-scale variability via kriging interpolation. Snow densities were distributed across the basin through regression analysis. Combining the modeled depths and densities with SCA produced spatially distributed SWE estimates near peak accumulation in 1997 and 1998.

---

[1]Department of Earth Resources, Colorado State University, Fort Collins, CO 80523
[2]Now at NWS Alaska River Forecast Center, 6930 Sand Lake Road, Anchorage, AK 99502

Paper presented at the Western Snow Conference, South Lake Tahoe, California, April, 1999.

FIELD METHODS

Study site

Loch Vale watershed (LVWS) lies in Colorado's Front Range immediately east of the Continental Divide at 40° 17' N, 105° 40' W (Figure 1). This glacially scoured basin in Rocky Mountain National Park has an area of approximately 6.9 km^2 and elevations between 3091 and 4003 m. The basin has a general east-northeast aspect and is flanked by steep cliffs on most margins. Slopes in the watershed range from a minimum of 0° to a maximum of 85° with a mean slope of 33°. Both Andrews Creek and Icy Brook drain the watershed and eventually flow into the Big Thompson River, a major tributary of the South Platte River. *Baron and Mast* [1992] provide a more detailed description of the watershed.

Field measurements

Intensive snow surveys were completed in LVWS during 15-18 April, 1997 and 7-10 April, 1998. Within the South Platte basin, the 1997 and 1998 snowpacks for the Big Thompson basin were respectively about 148% and 98% of the 30-year average for 1 May [*Colorado Basin Outlook Report*, 1997 and 1998]. Continuous wind-loading on steeper slopes during the 1998 snow survey prevented depth sampling in the higher drainages of LVWS. Therefore, there was less spatial coverage of depth measurements in 1998. Snow depths were measured at 197 points in 1997 and 173 points in 1998. Snow densities were measured in seven snowpits in 1997 and six snowpits in 1998. Sample depth and density locations were chosen to be representative of the range of elevations, slopes and aspects of the watershed, considering safety limitations. The sample locations for 1997 (Figure 2) were transcribed onto the USGS 7.5' McHenrys Peak Quadrangle, while the sample locations for 1998 were pinpointed on 5 m interval contour maps. The respective UTM coordinates were then obtained for each sampled site and registered to a 10 m resolution digital elevation model (DEM) of LVWS. The 5 m interval contour maps were derived directly from the 10 m DEM, which was constructed in August 1997.

Depth sample locations were predetermined from 50 m grids aligned orthogonal to the valley walls. At each depth sample location, a central measurement was taken with aluminum probe poles. Two additional depths were measured at 5 m spacing from the central point in directions aligned with the grid. To minimize local variation in depth, the three measurements were averaged and recorded to the nearest 0.05 m. However, to ensure adequate spatial coverage in the upper drainages, only one measurement was made at most sample points and the sampling was shifted to 100 m spacing due to probing difficulties and time constraints. The spacing between sample points was measured with probe poles. Snowpits were dug in the watershed to obtain density and temperature profiles. Densities were measured with a 1-L stainless steel wedge-shaped cutter and an electronic digital scale, or with a 0.25-L cutter and a spring scale. Continuous density profiles were sampled in 0.10 m increments on the shaded snowpit wall. The density samples were then averaged to obtain one representative density for each snowpit. Snowpit temperature profiles indicated the cold content of the snowpack had not been entirely removed as snowpack temperatures ranged from near 0°C to -9°C for 1997 and from near 0°C to –6.5°C for 1998. There was no significant snowmelt in LVWS before either snow survey.

MODELING METHODS

Binary decision trees

Binary decision trees relate independent variables with a dependent variable in a nonlinear or hierarchical manner through a series of binary decisions, or splits. A binary decision tree effectively delineates similar values of the dependent variable through a progressive subdivision of a heterogeneous sample. Based on a learning sample X containing a set of predictor variables and a response variable y, binary decision trees estimate values for y. A binary tree is grown by repeated splits of subsets of X into two descendent subsets or nodes. The splits begin with X itself, the root node, and end in a series of terminal nodes. At each node, the splits are conditionally chosen on values in a vector of independent variables, $\mathbf{x}$, (x_m, m=1,2,...) and based on the value of a single predictor variable in $\mathbf{x}$. Considering all possible parent nodes, the algorithm selects the split at a particular parent node that maximizes the reduction in total model deviance in y. Thus, the learning sample X is recursively partitioned to minimize model deviance in y. For a more detailed discussion of binary decision trees, refer to *Breiman et al.* [1984]. *Clark and Pregibon* [1992] provide details of the decision tree modeling software used in this study.

Binary decision trees offer many advantages over other methods used to distribute snow across mountainous terrain. The dependent variable, snow depth, is included in the model development through the stepwise reduction of model deviance. Decision trees can explain nonlinear relationships through multiple splits on the same independent variable. Unlike many multiple linear regression models, decision trees are easy to interpret. Individual splits can also be checked for physical justification. The major disadvantage associated with decision trees is the requirement of a large data set. Although the need for a large data set may hinder the widespread applicability of binary decision trees for modeling snow distribution, they have been found to be superior to most attempts to distribute snow over complex terrain [*Elder*, 1995].

Kriging

By modeling both spatial trend and spatial correlation, geostatistics offers a stronger approach to estimation procedures than classical statistics that assume variables are spatially independent and random. Relying on an explicit model of spatial variability, confirmed by the data set, geostatistical methods are reproducible, more objective and potentially more accurate than manual interpolation techniques. Geostatistics can be used to: (1) produce unbiased estimates of unknown quantities, (2) evaluate the reliability of the estimates, and (3) predict the effects on estimation accuracy of an additional set of measurements, as in the evaluation of proposed sampling networks [*Kitanidis*, 1993].

The variogram, a representation of the spatial variability, can be used to estimate the value of a variable $z(x_o)$ at a point x_o at which no data are available [*Journel and Huijbregts*, 1978]. This interpolation method, known as kriging, consists of three steps. The covariation of data values depending on their separation distance is examined. Theoretical models are then fit to these relationships. These models are finally used to calculate the weights for a particular set of neighboring measurements and to compute the interpolated value [*Phillips et al.*, 1992]. In theory, since it is an exact estimator yielding zero deviance at sampled points, kriging has an advantage over other interpolation schemes. Refer to *Balk et al.* [1998] for a more detailed description of kriging and its application to estimating snow distribution in LVWS.

Independent variables

Net solar radiation, elevation, slope and vegetation cover were used as physically based independent variables in our modeling attempts to spatially distribute SWE across LVWS. Net solar radiation has been shown to be a dominant energy source for melting alpine snowpacks [*Cline*, 1997] and plays a controlling role in the accumulation and redistribution of snow. *Elder* [1995] found that using a spatially distributed net solar radiation index over a portion of the snow accumulation season may be sufficient for statistical models of SWE distribution in alpine areas. Net solar radiation was modeled in Image Processing Workbench, **ipw** [*Frew and Dozier*, 1986], using the algorithm of *Dozier* [1980]. We applied the same radiation modeling efforts discussed by *Balk et al.* [1998], except a constant albedo of 0.25 was applied to snow-free areas. This snow-free albedo value proved sufficient in modeling efforts conducted by *Olyphant* [1986] in nearby alpine sites. Snow-covered and snow-free areas were determined using a mask of a SCA image of LVWS.

Elevation has been shown to be an important factor in snow distribution primarily through orographic effects [e.g., *Rhea and Grant*, 1974; *Caine*, 1975] and wind redistribution at the highest elevations. Elevations for this study were obtained from the 10 m DEM of LVWS, and vertical errors for the elevations were less than 1 m. Slope values were calculated for each grid cell in the DEM using an algorithm in ARC/INFO Ver. 7.2.1 geographic information system. Snow is often redistributed from steeper slopes to more gentle slopes through avalanching or sloughing. Avalanching does not change the total mass of SWE in a basin, but it does affect SWE distribution as large volumes of snow can be transported to and concentrated in lower elevation runout zones [*Elder et al.*, 1991; *de Scally*, 1996]. Vegetation type and size influence snow distribution through the interception of snowfall, subsequent losses due to evaporation, redistribution of snow, surface roughness, and surface energy exchange [e.g., *Steppuhn and Dyck*, 1974; *Adams*, 1976]. The vegetation coverage used in this study was simplified from a detailed vegetation classification for Rocky Mountain National Park. The vegetation classes include rock/alpine grassland, glacier, open water, spruce/fir and krummholz/willow. Glacier and open water are physiographic classes that have different snow accumulation patterns.

Dependent variables

Snow depth

Snow depths were distributed across LVWS with a combination of binary decision tree and geostatistical methods. The large-scale variability of snow depth was modeled with binary decision trees while the small-scale variability was modeled with kriging techniques. Rugged terrain, variable winds and complex radiation inputs contribute to the large heterogeneity in snow depth found in LVWS. This large heterogeneity in snow depth complicated initial modeling efforts of distributing snow depths by the kriging interpolation process alone [*Balk et al.*, 1998]. Binary decision trees can more accurately handle abrupt changes in the dependent variable, and thus were used to model the large-scale variations in snow depth. The estimated snow depths from the binary decision trees were then subtracted from the measured snow depths, and the resulting residuals were modeled through kriging interpolation. The modeled snow depths from the binary decision trees and modeled residuals from geostatistical techniques were then added together to produce estimates of the spatial distribution of snow depth.

Multiple binary decision trees were grown on the 1997 and 1998 data sets using tree-based model implementation in the S-Plus mathematical language [*Chambers and Hastie*, 1992]. For both years, binary decision trees were grown with various combinations of net solar radiation, elevation, slope and vegetation cover as independent variables. As a measure of the overall goodness of fit of each decision tree, the coefficient of determination (R^2) was calculated using standard statistical procedures. The default stopping criteria in the S-Plus mathematical language grew trees between 25 and 30 terminal nodes, prior to pruning. The best-fit decision tree model for snow depth in 1997 was grown with net solar radiation, elevation and slope. Using net solar radiation, elevation, slope and vegetation cover type yielded the best-fit tree model for 1998. Selection of the optimal binary decision trees for 1997 and 1998 was made through cross-validation and pruning. The 1997 and 1998 best-fit tree models were pruned to the respective upper range of terminal nodes determined through cross-validation. We further pruned these decision trees based on physical justification of the individual splits. The optimal decision trees for both years coincidentally had 18 terminal nodes. The 1998 optimal tree is shown in Figure 3.

The residuals from the binary decision tree models were spatially distributed across LVWS through kriging interpolation techniques conducted in S-Plus [*Chambers and Hastie*, 1992] with software developed by *Reich and Davis* [1998]. The residuals were estimated by ordinary kriging using only the primary variable, the residual depth. The residuals were also cokriged using net solar radiation, elevation and slope as separate auxiliary variables. Interpolations were made at 10 m intervals to correspond with the 10 m DEM. Experimental variograms and cross-variograms were constructed with maximum distance parameters and a certain number of distance classes, or bins, to best represent the spatial variability of the residuals, auxiliary variables and their interactions. A stationarity assumption was made where the means and variances of each regionalized variable were assumed to be independent of location and constant throughout the watershed. Isotropic variance structure was also assumed for each regionalized variable since no significant directional differences in the experimental variograms were found. The experimental variograms were then fit with Gaussian, spherical and exponential variogram models. The best-fit theoretical variograms used in the kriging interpolations were selected through ordinary least-squares regression. The experimental variograms and theoretical spherical model fits for 1997 radiation and 1998 residual depths are shown in Figure 4.

Cross-validation was used to evaluate the statistical properties of the kriged and cokriged surfaces and to determine the ideal number of nearest neighbors, or residual values, to be used in each model. Each observed residual depth, z_i, was suppressed in turn, and its value was predicted from the remaining data using the selected theoretical variogram. The observed residual depths minus the estimated residual depths yielded a new set of residuals, hereafter referred to as the residual errors. These residual errors were analyzed to evaluate the underlying model assumptions. All models had approximately normally distributed residual errors with a mean of zero and constant variance. To assess the overall goodness of fit of each model, the coefficient of determination (R^2) was calculated by:

$$R^2 = 1 - \frac{\sum_{i=1}^{n}\left(\varepsilon_i - \bar{\varepsilon}\right)^2}{\sum_{i=1}^{n}\left(z_i - \bar{z}\right)^2} \qquad (1)$$

where ε_i is the residual error associated with the response variable, z_i [*Reich and Davis*, 1998]. This R^2 value has an upper limit of one and no lower limit. A negative R^2 value indicates the variance in errors of the kriging model is larger than the variance in the observed data.

Snow density

Since density varies less than depth in alpine areas [*Logan*, 1973], measurements from a few snowpit density profiles are sufficient and can be spatially distributed across the watershed through regression analysis. Net solar radiation, elevation and slope were considered as independent variables in snow density modeling. Elevation and slope did not show a significant relationship with snow density; therefore, only an index of net solar radiation was used to model density. For 1997, a general linear model explaining 47% of the observed variance in field measurements of snow density was used to distribute density ($R^2 = 0.466$, n = 7, p = 0.091). A general linear model explaining 80% of the observed variance in 1998 sampled densities was used to distribute density for that year ($R^2 = 0.796$, n = 6, p = 0.017). These general linear models proved sufficient and were more ideal than merely applying a mean density that would ignore the observed spatial variations in density.

Snow-covered area

Using high-resolution aerial photographs of LVWS taken on 9 April, 1996, the SCA for LVWS was calculated to be 56% of the watershed area [*Balk et al.*, 1998]. Due to the extreme topography and dry continental snowpack of LVWS, most of the steeper slopes in the watershed cannot maintain snow cover, even during heavy snowfall years. Therefore, it is assumed that snow cover near peak accumulation will be fairly consistent from year to year. In the final snow-covered image, areas with no snow were assigned a zero value, while areas with snow cover were assigned a value of one.

RESULTS

Snow depth

Considering the heterogeneous snow distribution found in complex alpine terrain, the model results proved favorable. The results for the 1997 tree ($R^2 = 0.539$) and the 1998 tree ($R^2 = 0.648$) are similar to the results found for other alpine basins [*Elder*, 1995; *Elder et al.*, 1998]. The higher R^2 value for the 1998 tree is probably the result of more accurate registration of the sample points to the DEM. For the 1997 and 1998 kriged residual models, all R^2 values were less than zero. The negative R^2 values indicate that the kriged surface is less useful for modeling the residuals than the original surface, i.e., no additional information is gained by kriging the residuals. With the poor results of the kriged surfaces, subsequent analysis only considered the cokriging models. The radiation and slope cokriging models had similar R^2 values for various nearest neighbors. However, the radiation cokriging models were chosen since radiation tends to exhibit a stronger correlation with snow distribution.

Combining the decision tree-modeled depths with the radiation cokriged estimates of the residuals offers improvement on the tree-modeled depth surface. The R^2 values for the final depths were calculated by subtracting from one the variance that is still unexplained by the combined models. The R^2 values are essentially calculated using (1) except here the response variable, z_i, refers to the measured snow depths. The final depths explained 60-85% of the observed variance in measured depths (Figure 5). Summaries of field measured depths and modeled depths using two nearest neighbors in the interpolation process are given in Table 1. Statistics were computed for only the snow-covered areas in the "SCA" model, whereas the "Basin" model statistics were generated for the entire watershed. Since interpolations were made at 10 m intervals and did not correspond precisely with the sampled locations, the estimated residual depths often did not correspond to the observed residual depths. With nugget effects present, the variograms are discontinuous at zero distance and the kriged or cokriged estimate at a small distance from a sampled location can be quite different than the sampled measurement [*Kitanidis*, 1993].

Table 1. Summary of field measured and model estimated snow depths where standard deviation (σ), coefficient of variation (C.V.), and sample size (n) are included. Sample size for modeled depths is the total number of 10 m cells, where "SCA" denotes snow-covered areas in LVWS and "Basin" denotes the entire watershed. Modeled depths are from the two nearest neighbor combined models.

Depth	Min (m)	Max (m)	Mean (m)	σ (m)	C.V.	n
1997 measured	0.05	10.25	3.03	2.13	0.70	197
1997 modeled, SCA	0	11.90	4.46	2.53	0.57	39022
1997 modeled, Basin	0	11.90	2.52	NA	NA	69188
1998 measured	0.05	6.05	2.09	1.41	0.67	173
1998 modeled, SCA	0	6.05	2.39	1.17	0.49	39022
1998 modeled, Basin	0	6.05	1.35	NA	NA	69188

Snow water equivalence

Estimates of SWE distribution for each year were calculated by multiplying the combined depth surfaces by the modeled density and SCA map. The 1997 and 1998 SWE distributions were generated using two to seven nearest neighbors in the cokriging interpolation of the depth residuals. This range of nearest neighbors was chosen because it represented the highest R^2 values of the 1997 and 1998 combined depth models (Figure 5). Hereafter, these models will be referred to as SWEYY_N, where YY denotes the year and N denotes the number of nearest neighbors. For example, SWE97_6 refers to the 1997 model with six nearest neighbors. Quantitative comparisons between final SWE distributions were referenced to the SWE97_2 and SWE98_2 maps. These SWE maps had the highest model fit of snow depth (Figure 5). Expressed as depths, SWE values for SWE97_2 and SWE98_2 are summarized in Table 2, where "SCA" and "Basin" have the same meanings as above.

Table 2. Summary of modeled SWE expressed as depth from the two nearest neighbor combined models where standard deviation (σ), coefficient of variation (C.V.), and sample size (n) are included. Sample size is the total number of 10 m cells, where "SCA" denotes snow-covered areas in LVWS and "Basin" denotes the entire watershed.

SWE Model	Min (m)	Max (m)	Mean (m)	σ (m)	C.V.	n
1997, SCA	0	4.20	1.55	0.84	0.54	39022
1997, Basin	0	4.20	0.88	NA	NA	69188
1998, SCA	0	1.95	0.72	0.34	0.47	39022
1998, Basin	0	1.95	0.41	NA	NA	69188

For the two through seven nearest neighbor SWE maps, the mean SWE depth, $\overline{SWE}$, and total SWE volume, SWE_{tot}, are shown in Table 3. As an indicator of SWE distribution differences, the total SWE volume displaced, SWE_{disp}, between two model surfaces was calculated by:

$$SWE_{disp} = \sum_{i=0}^{M}\sum_{j=0}^{N}\left[\left(SWE_{xij} - SWE_{yij}\right)^2\right]^{1/2} \qquad (2)$$

where SWE_x and SWE_y are model values at cell locations i,j for an M by N grid [*Elder*, 1995]. Displaced SWE volumes calculated between the two nearest neighbor SWE map and the three through seven nearest neighbor SWE maps are indicated in Table 3.

Table 3. Summary of modeled SWE for 1997 and 1998. $\overline{SWE}$ represents mean SWE expressed as depth for the basin. SWE_{tot} represents total SWE in the basin. SWE_{disp} refers to the displaced SWE in the basin calculated between the two nearest neighbor model and the three through seven nearest neighbor models.

Model	$\overline{SWE}$ (m)	SWE_{tot} Volume (m^3)	ΔSWE_{tot} % from SWEYY_2	SWE_{disp} Volume (m^3)	ΔSWE_{disp} % from SWEYY_2
SWE97_2	0.88	6,050,000	NA	NA	NA
SWE97_3	0.86	5,950,000	1.7	657,000	10.9
SWE97_4	0.85	5,900,000	2.5	789,000	13.0
SWE97_5	0.85	5,870,000	3.0	899,000	14.9
SWE97_6	0.85	5,860,000	3.1	962,000	15.9
SWE97_7	0.85	5,870,000	3.0	1,010,000	16.7
SWE98_2	0.41	2,810,000	NA	NA	NA
SWE98_3	0.40	2,790,000	0.7	353,000	12.6
SWE98_4	0.40	2,750,000	2.1	443,000	15.8
SWE98_5	0.40	2,730,000	2.8	484,000	17.2
SWE98_6	0.39	2,730,000	2.8	512,000	18.2
SWE98_7	0.40	2,750,000	2.1	519,000	18.5

DISCUSSION

Snow depth

The 1997 and 1998 decision trees generate a mosaic of discrete depth classes that effectively capture the abrupt changes in snow depth. A kriged or cokriged depth surface tends to smooth the large-scale variations in depth and nullify the natural heterogeneity [*Balk et al.*, 1998]. The averaging of positive and negative residual depths over larger areas reduces the impact of increasing the number of nearest neighbors. The cokriged residual models do not gain additional information from more than seven nearest neighbors. This averaging effect is believed to cause the R^2 values to decrease asymptotically (Figure 5). The binary decision trees sufficiently modeled abrupt large-scale variations in depth, highlighting a mosaic of wind-scoured and depositional areas. By adding the cokriged residual surfaces to the tree models, the transitions between areas of high and low accumulations are smoothed. We feel the combined model depth surfaces sufficiently represent the snow depth surfaces found in the field.

Snow water equivalence

The SWE97_2 and SWE98_2 maps are shown in Figures 6 and 7 respectively. Figures 6 and 7 show relatively high SWE accumulations in the sheltered Andrews Creek subbasin and relatively low SWE accumulations in the broader Sky Pond subbasin. Noticeable elevation banding of SWE is present in the SWE97_2 map. This banding reflects elevation as the dominant split in the 1997 decision tree of snow depth. Of note in the SWE98_2 map is the lack of higher SWE values around Andrews Glacier, at the headwaters of Andrews Creek. The lower SWE values around Andrews Glacier can be explained by the inability to sample that region during the survey. Andrews Glacier is expected to have large seasonal deposits of SWE [*Outcalt*, 1965]. The few depth samples taken at high elevations in the Sky Pond subbasin were not representative of the conditions, particularly depth and radiation, around Andrews Glacier. Thus, the 1998 decision tree had difficulty modeling the snow distribution in this area.

The changes in SWE_{tot} between the two nearest neighbor SWE map and the other maps are less than 3.1% (Table 3). These small differences indicate that all combined models estimate similar volumes of snow. However, the large changes in SWE_{disp}, 10.9-18.5% (Table 3), suggest a larger change in distribution of snow between the SWE maps. Such snow distribution differences have little effect on SWE_{tot} estimates, but may have important implications in snowmelt modeling. For example, the model relocation of 15% of the total snow volume to areas receiving greater amounts of incoming radiation may substantially alter the resultant snowmelt hydrograph both in terms of timing and peak runoff.

CONCLUSIONS

Difficulties were encountered in modeling efforts to interpolate snow depths across LVWS through kriging interpolation alone [*Balk et al.*, 1998]. These complications motivated interest to model the large-scale variations in snow depth with binary decision trees and the small-scale variations through geostatistical techniques. The combined models of snow depth are improvements over using decision tree or geostatistical methods alone to estimate snow distribution in complex mountain environs. Between 60 and 85% of the observed variance in depth measurements was explained by the combined models of snow depth. Binary decision trees delineate similar snow accumulations by relating snow depth with independent variables based on topography, energy balance and vegetation. By modeling depth in a nonlinear, hierarchical fashion, decision trees can detect the abrupt changes in snow depth found in heterogeneous mountain snowpacks. Using net solar radiation as an auxiliary variable, cokriging interpolation of the residuals effectively smoothes the transitions between these abrupt changes in depth. Estimating the residual depths with ordinary kriging did not provide additional information to the decision tree models. Through regression analysis, snow densities were spatially modeled through LVWS. The combination of the final depth surfaces, modeled densities and SCA delivered spatially distributed estimates of SWE. Such spatial estimates of SWE are necessary for accurate prediction of the magnitude and timing of snowmelt runoff.

Acknowledgments

Jill Baron, USGS/BRD, provided financial and editorial assistance. Don Campbell, George Ingersoll and numerous other USGS personnel from Denver, along with Joe Stock, Eric Allstott and Doug Bopray provided help with the snow surveys. Robin Reich assisted with geostatistical modeling efforts. Adam Winstral provided the program to map binary decision tree output. Don Cline, NOAA/NOHRSC, coordinated the pre-processing of the aerial photos used to construct the 10 m DEM of LVWS and the SCA map. Ralph Root and Larry Fairbank, USGS/BRD, Center for Biological Informatics, provided assistance in constructing the DEM. This research was funded by the Colorado Rockies Global Climate Change Program, USGS, Loch Vale Watershed project.

REFERENCES

Adams, W., Areal differentiation of snow cover in East Central Ontario, *Water Resources Research, 12*, 1226-1234, 1976.

Balk, B., K. Elder, and J. Baron, Using geostatistical methods to estimate snow water equivalence distribution in a mountain watershed, *Proceedings of the Western Snow Conference, 66*, 100-111, 1998.

Baron, J., and M. A. Mast, Regional characterization and setting for the Loch Vale Watershed study, in *Biogeochemistry of a Subalpine Ecosystem: Loch Vale Watershed*, edited by J. Baron, pp. 12-27, Springer-Verlag, New York, 1992.

Blöschl, G., R. Kirnbauer, and D. Gutknecht, Distributed snowmelt simulations in an alpine catchment, 2, Parameter study and model predictions, *Water Resources Research, 27*(12), 3181-3188, 1991.

Breiman, L., J. Friedman, R. Olshen, and C. Stone, *Classification and Regression Trees*, Wadsworth and Brooks, Pacific Grove, Calif., 1984.

Caine, N., An elevational control of peak snowpack variability, *Water Resources Bulletin, 11*, 613-621, 1975.

Chambers, J., and T. Hastie (eds.), *Statistical Models in S*, Wadworth and Brooks, Pacific Grove, Calif., 1992.

Clark, L., and D. Pregibon, Tree-based models, in *Statistical Models in S*, edited by J. Chambers and T. Hastie, pp. 377-419, Wadsworth and Brooks, Pacific Grove, Calif., 1992.

Cline, D. W., Snow surface energy exchanges and snowmelt at a continental, midlatitude Alpine site, *Water Resources Research, 33*(4), 689-701, 1997.

Cline, D. W., R. C. Bales, and J. Dozier, Estimating the spatial distribution of snow in mountain basins using remote sensing and energy balance modeling, *Water Resources Research*, *34*(5), 1275-1285, 1998.

Colorado Basin Outlook Report, May 1, Natural Resource Conservation Service, Lakewood, Colo., 1997.

Colorado Basin Outlook Report, May 1, Natural Resource Conservation Service, Lakewood, Colo., 1998.

de Scally, F. A., Avalanche snow melting and summer streamflow differences between high-elevation basins, Cascade Mountains, British Columbia, Canada, *Arctic and Alpine Research*, *28*(1), 25-34, 1996.

Doesken, N. J., and A. Judson, *The Snow Booklet: A Guide to the Science, Climatology, and Measurement of Snow in the United States*, Colorado State University Department of Atmospheric Science, Fort Collins, Colo., 1996.

Dozier, J., A clear-sky spectral solar radiation model for snow-covered mountainous terrain, *Water Resources Research*, *16*, 709-718, 1980.

Elder, K., Snow distribution in alpine watersheds, Ph.D. dissertation, 309 pp., Univ. of Calif., Santa Barbara, 1995.

Elder, K., J. Dozier, and J. Michaelsen, Snow accumulation and distribution in an alpine watershed, *Water Resources Research*, *27*, 1541-1552, 1991.

Elder, K., W. Rosenthal, and R. E. Davis, Estimating the spatial distribution of snow water equivalence in a montane watershed, *Hydrological Processes*, *12*, 1793-1808, 1998.

Frew, J., and J. Dozier, The Image Processing Workbench – portable software for remote sensing instruction and research, in *Proceedings IGARSS '86*, ESA SP-254, pp. 271-276, European Space Agency, Paris, 1986.

Hosang, J., and K. Dettwiler, Evaluation of a water equivalent of snow cover map in a small catchment area using a geostatistical approach, *Hydrological Processes*, *5*, 283-290, 1991.

Journel, A. G., and Ch. J. Huijbregts, *Mining Geostatistics*, 600 pp., Academic Press, New York, 1978.

Kitanidis, P. K., Geostatistics, in *Handbook of Hydrology*, edited by D. R. Maidment, pp. 20.1-20.39, McGraw-Hill, New York, 1993.

Logan, L. A., Basin-wide water equivalent estimation from snowpack depth measurements, in *Role of Snow and Ice in Hydrology*, *IAHS Publ. 107*, 864-884, 1973.

Olyphant, G. A., The components of incoming radiation within a mid-latitude alpine watershed during the snowmelt season, *Arctic and Alpine Research*, *18*(2), 163-169, 1986.

Outcalt, S. I., The regimen of the Andrews Glacier in Rocky Mountain National Park, Colorado, 1957-1963, *Water Resources Research*, *1*(2), 277-282, 1965.

Phillips, D. L., J. Dolph, and D. Marks, A comparison of geostatistical procedures for spatial analysis of precipitation in mountainous terrain, *Agricultural and Forest Meteorology*, *58*, 119-141, 1992.

Reich, R. M., and R. Davis, *Quantitative Spatial Analysis NR/ST523 Course Notes*, 422 pp., Colorado State University, Fort Collins, Colo., 1998.

Rhea, J. O., and L. O. Grant, Topographic influences on snowfall patterns in mountainous terrain, in *Advanced Concepts and Techniques in the Study of Snow and Ice Resources*, pp. 182-192, National Academy of Sciences, Washington, DC, 1974.

Steppuhn, H., and G. Dyck, Estimating true basin snow cover, in *Advanced Concepts and Techniques in the Study of Snow and Ice Resources*, pp. 314-328, National Academy of Sciences, Washington, DC, 1974.

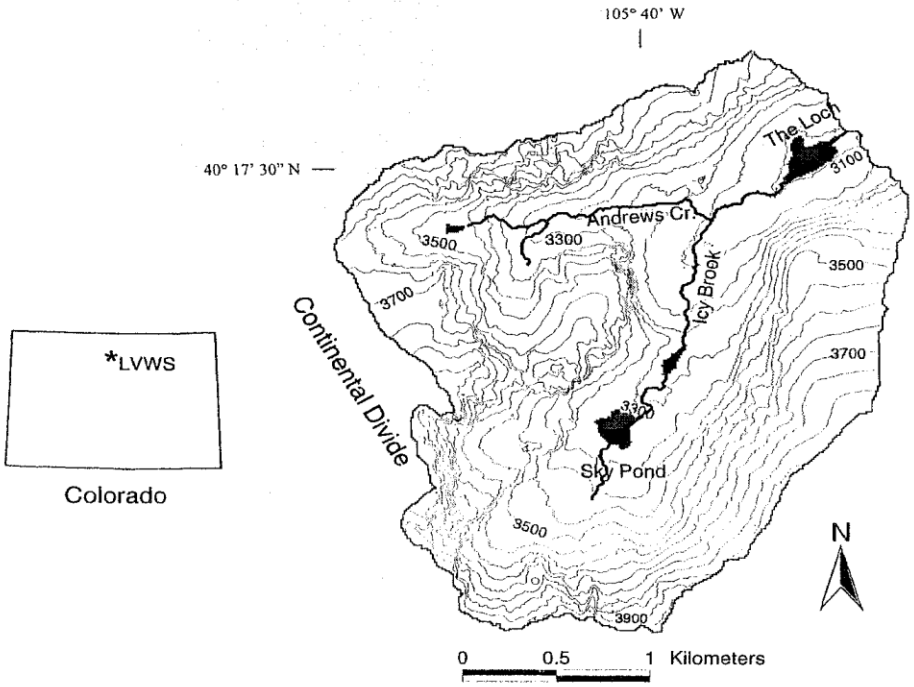

Figure 1. Location and topographic map of the Loch Vale watershed (LVWS). Contour interval is 50 meters.

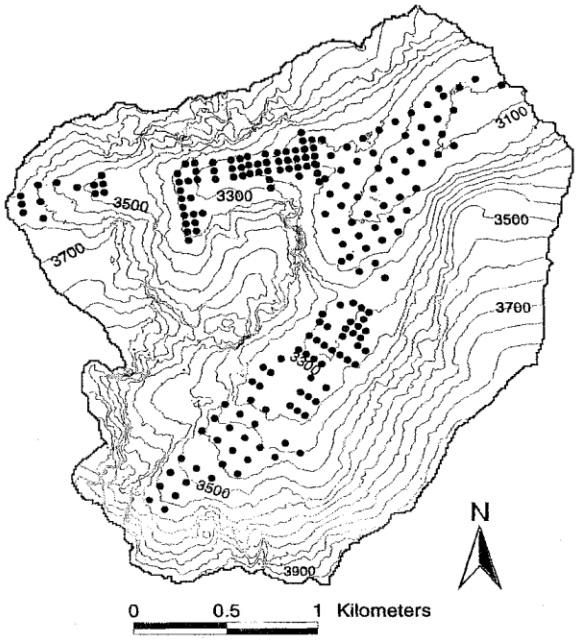

Figure 2. 1997 depth sampling sites (n = 197) indicated with dots. Contour interval is 50 meters.

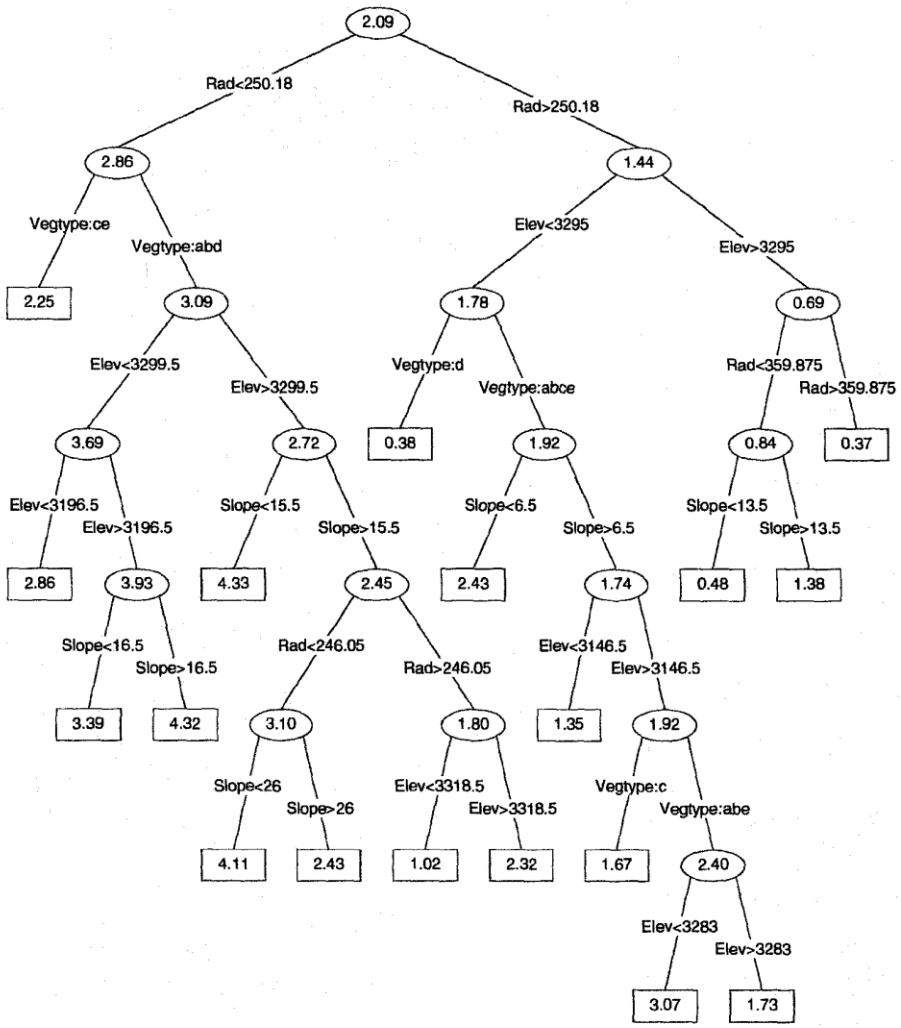

Figure 3. Binary decision tree for 1998 measured snow depths. Values in each node are mean depths (m) for all members in that node. Vegetation type classifications: a-glacier; b-rock/alpine grassland; c-spruce/fir; d-open water; e-krummholz/willow.

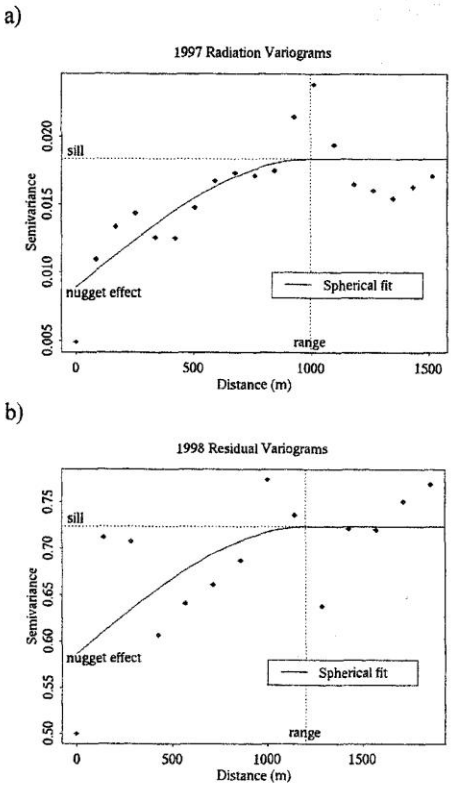

Figure 4. Experimental variograms and spherical theoretical models for (a) 1997 radiation and (b) 1998 residuals (measured depth – tree-modeled depth). The nugget effect, sill and range are identified.

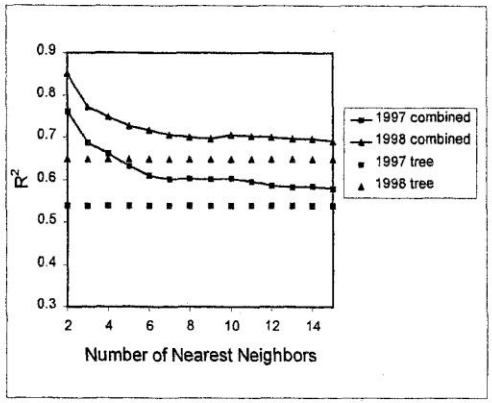

Figure 5. Snow depth models. Coefficient of determination (R^2) versus number of nearest neighbors used in cokriging the residuals. Solid lines with symbols indicate combined models of snow depth (i.e., cokriged estimates of residuals added to the tree-modeled depths). Horizontal rows of symbols indicate R^2 values for only the binary decision tree models.

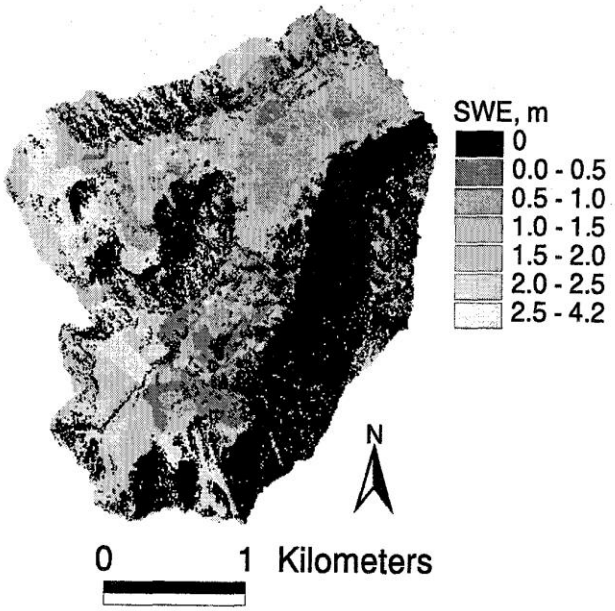

Figure 6. Combined model snow water equivalence expressed as depth for 1997 (SWE97_2). Dark regions indicate shallow SWE accumulations; bright regions indicate deeper SWE accumulations. Depths are shown in meters.

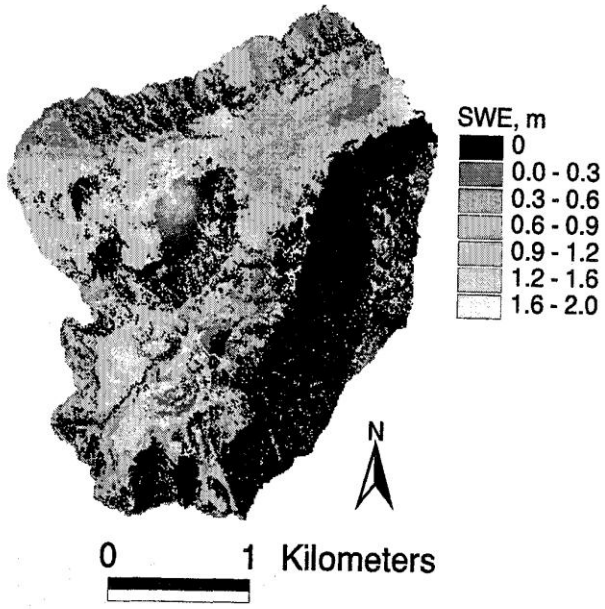

expressed as depth for 1998 (SWE98_2). Dark regions indicate shallow SWE accumulations; bright regions indicate deeper SWE accumulations. Depths are shown in meters.